DOI: 10.1002/chem.200500275

Monodisperse Oligofluorenes with Keto Defect as Models to Investigate the Origin of Green Emission From Polyfluorenes: Synthesis, Self-Assembly, and Photophysical Properties**

Chunyan Chi, Chan Im, Volker Enkelmann, Andreas Ziegler, Günter Lieser, and Gerhard Wegner*[a]

Abstract: Oligofluorenes (a trimer, pentamer, and heptamer) with one fluorenone unit in the center (**OF*n*K**: $n=3$, 5, or 7) were synthesized and used as models to understand the origin of the low-energy emission band in the photoluminescence and electroluminescence spectra of some polyfluorenes. All compounds form glasses with T_g at 30 °C (**OF3K**), 50 °C (**OF5K**) and 57 °C (**OF7K**). Oligomers **OF5K** and **OF7K** exhibit smectic liquid crystal phases that undergo transition to isotropic melts at 107 and 205 °C, respectively. Oligomer **OF5K** could be obtained in form of single crystals. The X-ray structure analysis revealed the helical nature of the molecule and a helix reversal defect located at the central fluorenone unit. The packing pattern precludes formation of excimers. Electrochemical properties were investigated by cyclic voltammetry. The ionization potential (I_p) and electron affinity (E_a) were calculated from these data. Studies of the photophysical properties of **OF*n*K** in solution and thin film by steady-state and time-resolved fluorescence spectroscopic measurements suggest efficient funneling of excitation energy from the photoexcited fluorene segments to the low-energy fluorenone sites by both intra- and intermolecular hopping events whereby they give rise to green emission. Intermolecular energy transfer was investigated by using a model system composed of a highly defect free polyfluorene **PF2/6** doped by **OF*n*K**. Förster-type energy transfer takes place from **PF2/6** to **OF*n*K**. The energy-transfer efficiency increases predictably with increasing concentration of **OF*n*K**.

Keywords: conjugation · energy transfer · liquid crystals · oligomers · photophysics · polyfluorenones

Introduction

In the development of polymer light-emitting diodes (LEDs), blue-light emission is of particular importance.[1] Among the limited number of conjugated polymers that have been identified as promising materials for polymer LEDs emitting blue light, the 9,9-disubstituted poly(2,7-fluorene)s (PFs) exhibit high quantum efficiencies in photoluminescence (PL) and electroluminescence (EL).[2] High EL brightness can be achieved at acceptable thermal stability.[1c,d] Since all of these physical parameters can be optimized by chemical modification and copolymerization, the whole family of polymers has received interest as materials for blue-emitting LEDs and displays.[3] Moreover, PFs can also serve as host material, and the full gamut of colors (blue, green, and red) can be produced through energy transfer to longer wavelength emitters in blends with other conjugated polymers and/or with phosphorescent dyes.[4] A significant drawback that presents widespread application is the lack of stability of the polymers during operation of the light-emitting diodes (PLEDs).[5] Photooxidation plays an important role in the lifetime of PLEDs fabricated from conjugated polymers.[6] Most of PLEDs prepared from PFs suffer from degradation and consequently loss of efficiency under operation, which is most visibly documented in the formation of a low energy emission band in the "green" at 2.2–2.4 eV (520–560 nm). As a result, the desired blue emission shifts towards blue-green (and even yellow).[2] This un-

[a] Dr. C. Chi, Dr. C. Im, Dr. V. Enkelmann, Dr. A. Ziegler, Dr. G. Lieser, Prof. G. Wegner
Max Planck Institute for Polymer Research
Ackermannweg 10, 55128 Mainz (Germany)
Fax: (+49) 6131-379-100
E-mail: wegner@mpip-mainz.mpg.de

[**] Editorial note: Please also see the preceding paper, which is on a similar subject.

Supporting information for this article is available on the WWW under http://www.chemeurj.org/ or from the author. Synthesis and characterization of compounds, Schlieren texture image, additional photophysical spectra, and other experimental details.

desired long wavelength emission is observed[7] after both thermal- and photooxidation of the polymer in both PL and EL spectra, but it is typically more intense in the latter.[8] The origin of the additional green emission band has been controversially discussed. Initially, the long wavelength ("green") emission had been attributed to spontaneous formation of aggregates in the ground state and/or excimer formation that is aggregates in the photoexcited state.[9]

Following this line of thinking several attempts have been made to stabilize the blue emission of PFs by means of a chemical modification that would prevent the pairing of the chromophores by steric hindrance. Modifications including addition of bulky side groups,[9f,10] bulky end groups,[11] copolymerization (including incorporation of benzothiadiazole, perylene, and anthracene moieties into the PF main chain and through end-capping),[1i,12] dendronization,[13] and blending[3,14] have been tried. None of these approaches has succeeded to satisfactorily prevent or suppress the green EL. Pure blue emission was obtained from PF-based LEDs doped with a small concentration of hole-transporting (HT) molecules.[3,15] However, in such blends the device stability is limited by slow phase-separation. Thus, it remains a challenge to create long-lived, pure blue EL from PF-based LEDs.

However, an alternative explanation was recently put forward, claiming that emission from isolated fluorenone-type defects in polyfluorene chains rather than intermolecular aggregates or excimers are responsible for the emission in the green band. It was proposed that these fluorenone moieties are formed either from defects already present in the polymer when monoalkylated fluorenes were present as impurities during polymerization and became incorporated into the polymer, or later by thermal-, photo-, or electrooxidative degradation processes of almost any PFs,[16] for example, 9,9-dialkylated polyfluorenes (DA-PF). The main evidence for this suggestion was the observation of 1) the green emission band in very dilute solutions of fluorene oligomers and polymers[16c] and fluorenone-containing copolymers,[16d] 2) the lack of any significant concentration dependence of the green emission band in solutions of fluorenone-containing copolymers, and 3) the pronounced vibronic structure of the green emission band from thin films of fluorenone–fluorene copolymers at low temperatures.[16d] The tendency of 9-monoalkyl polyfluorenes (MA-PF) to undergo facile autoxidation is a proven fact. Pristine 9-monoalkylated MA-PF was already found to contain 9-fluorenone defect sites after polymer synthesis.[16a]

The incorporation of the fluorenone defect sites in MA-PF dramatically changes the emission properties of the polymer. The low-energy emission ("green") band is dominant in the emission spectra. The energetic position of the low-energy emission band at about 2.3 eV in MA-PF is very similar to the low-energy emission band of the fluorenone building block in statistical dialkylfluorene/fluorenone copolymers.[17,18]

It is also similar to the emission band of photooxidized (photodegradated) fluorene-endcapped poly(9,9-dihexylfluorene-2,7-diyl) (PF6) as demonstrated in the literature.[7,19] In this light, the often favored interpretation that the low-energy emission band in PF is associated with aggregate or excimer formation is at the very least questionable. A recent study which used a "trimer" (2,7-bis(2′-9′,9′-dihexylfluorenyl)-9-fluorene) with a keto group in the central unit also came to the conclusion that the green emission originates from the keto defect site.[20] However, in this report, structural data indicating the geometry of the oligomer in the ground state and the fact that the higher oligomers exhibit liquid crystallinity was missed.

It is interesting to note that the contribution of keto defect sites to the emission is more pronounced in electroluminescence when compared to photoluminescence.[21] The reason behind this observation is the presence of two simultaneous processes that contribute to the low-energy emission: 1) energy transfer from the singlet excitons on the PF main chain to keto defect sites and 2) trapping of charge carriers at the fluorenone defect sites followed by subsequent emissive recombination events. The second process is improbable in PL experiments and increases the contribution of the defect-site-related low-energy EL band in the EL experiment.

Further, recent theoretical studies taking fluorenone-containing oligomers into account substantiate the view that the green emission originates from the fluorenone moieties as a consequence of efficient energy transfer to these sites and strong localization of the excitons on the fluorenone units.[22]

As a contribution to this ongoing discussion and with the aim to understand better the mechanisms of color change of the emission owing to degradation,[2,23] highly pure monodisperse oligofluorenes (trimer, pentamer, and heptamer) with keto defects incorporated in the center of the molecule are used as models to pinpoint the origin of the green emission. Their electronic properties studied by UV-visible spectroscopy and cyclic voltammetry will be discussed in the following together with their photophysical properties, which were investigated by steady-state and time-resolved fluorescence measurements both on the pure oligomers and their blends with the corresponding poly(9,9-bis(2-ethylhexyl)fluorene-2,7-diyl) (**PF2/6**). Their thermal behavior and structure in the bulk were also studied by differential scanning calorimetry (DSC), polarized optical microscopy (POM), and single-crystal structure analysis.

Results and Discussion

Synthesis: The synthesis of the oligofluorenes with a central fluorenone unit is shown in Scheme 1. The monobromides of the fluorenyl monomer, dimer, and trimer (**1a**–**c**) with 2-ethylhexyl side chains in the 9-position of the fluorene unit were prepared according to our previous report.[24] This substitution pattern was chosen to ensure complete miscibility with the corresponding polyfluorene. The palladium-catalyzed Miyaura reaction[25] was used to transform the bromides to the boronates (**2a**–**c**) in high yield. The target

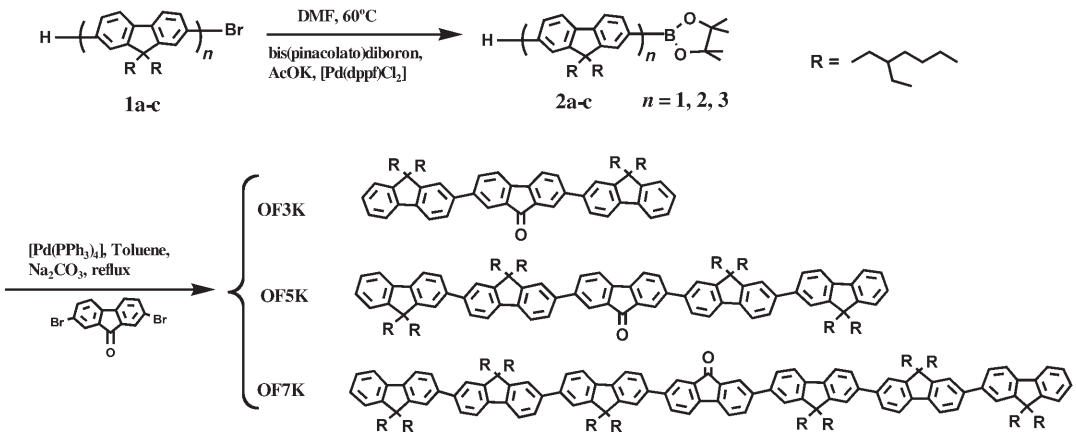

Scheme 1. The synthesis of oligofluorenes with central fluorenone unit.

products namely trimer, pentamer, and heptamer (**OF3K**, **OF5K**, and **OF7K**, respectively) with one fluorenone unit in the center were then prepared by Suzuki coupling between the monoboronate fluorenyl oligomers **2a–c** with 2,7-dibromofluorenone. All compounds were purified by standard column chromatography and their structure was confirmed by field desorption mass spectrometry (FD-MS) and ^{1}H or ^{13}C NMR spectra (see Figures 1–4 in the Supporting Information).

Thermal behavior and crystal structure: The thermal stability of the oligofluorenes with one fluorenone group is similar to that of homo-oligofluorenes.[24,26] The thermal gravimetric analysis (TGA) of **OF3K**, **OF5K**, **OF7K** under nitrogen does not show a change in mass up to 370 °C. The DSC traces (measured in a nitrogen atmosphere) shown in Figure 1 clearly exhibit the glass transition for all of the oligomers **OF3K** (29.8 °C), **OF5K** (49.8 °C), and **OF7K** (57.1 °C), followed by an endothermic transition for **OF5K** (106.8 °C) and **OF7K** (204.6 °C) upon heating. The latter is identified as a transition from the liquid crystalline phase to the isotropic melt, as was confirmed by polarized optical microscopy. Thin films of **OF5K** and **OF7K** exhibit typical Schlieren patterns (see Figure 5 in the Supporting Information), which could be observed during slow cooling from the isotropic phase. The Schlieren texture as well as the very small enthalpy of transition (ΔH_{iso} is $-0.74\,J\,g^{-1}$ for **OF5K**, $-0.77\,J\,g^{-1}$ for **OF7K**) are consistent with the occurrence of a smectic liquid crystalline phase.

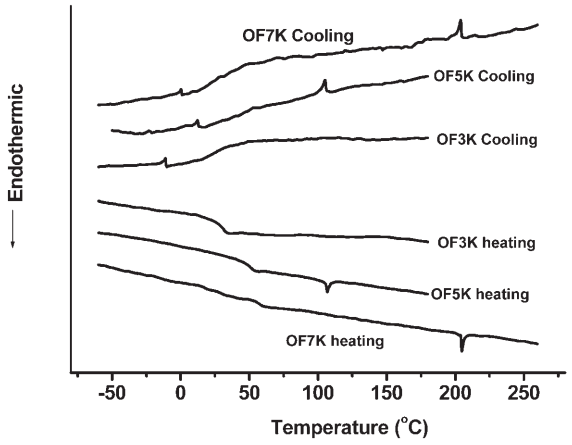

Figure 1. DSC traces of **OF3K**, **OF5K**, and **OF7K** (second heating and cooling at $10\,K\,min^{-1}$).

Single crystals of the pentamer **OF5K** were obtained from a solution of the sample in dichloromethane by slow dilution with ethanol. The material crystallizes in a monoclinic unit cell ($P2_1/c$) with $a=23.40$, $b=19.07$, $c=24.32$ Å; $\alpha=90$, $\beta=94.90$, $\gamma=90°$; $Z=4$, $V=10810.9$ Å^3, and $\rho_{calcd}=1.15\,g\,cm^{-3}$. As this point we need to recall that as-synthesized **OF5K** is actually a mixture of stereo isomers, since a racemic mixture of 2-ethylhexyl bromides was employed in the synthesis of the monomer fluorene derivative. The resulting and inherent disorder in the side-chain region of the oligomers enhances their solubility without disturbing the electronic properties. We did not attempt to separate the isomers and, in fact, the mixture of isomers undergoes crystallization without fractionation. However, the disorder in the side-chain region has the consequence that the ratio of observed over possible reflections amounts to roughly 0.1.[27] The number of strong and independent reflections is large enough to resolve the structure of the backbone with confidence, while the presence of the side chains is only seen as an electron density cloud. The conformation of the backbone alone is shown in Figure 2A as a projection onto the plane of the central fluorenone group. A helixlike structure is observed with rotation angles between adjacent fluorenyl elements near 144°; this is being the ideal value expected for the 5_2-helix that was identified as the structural element in the crystalline polymer **PF2/6**.[28] However, this conformation is disrupted in the vicinity of the fluorenone group, that is, between ring 3 and ring 4 the rotation is reversed. The reason for this type of conformational defect associated to the chemical defect in terms of the fluorenone group is unknown.

Figure 2B shows a projection of the crystal structure onto the *ac* plane. The precise position of the side chain segments

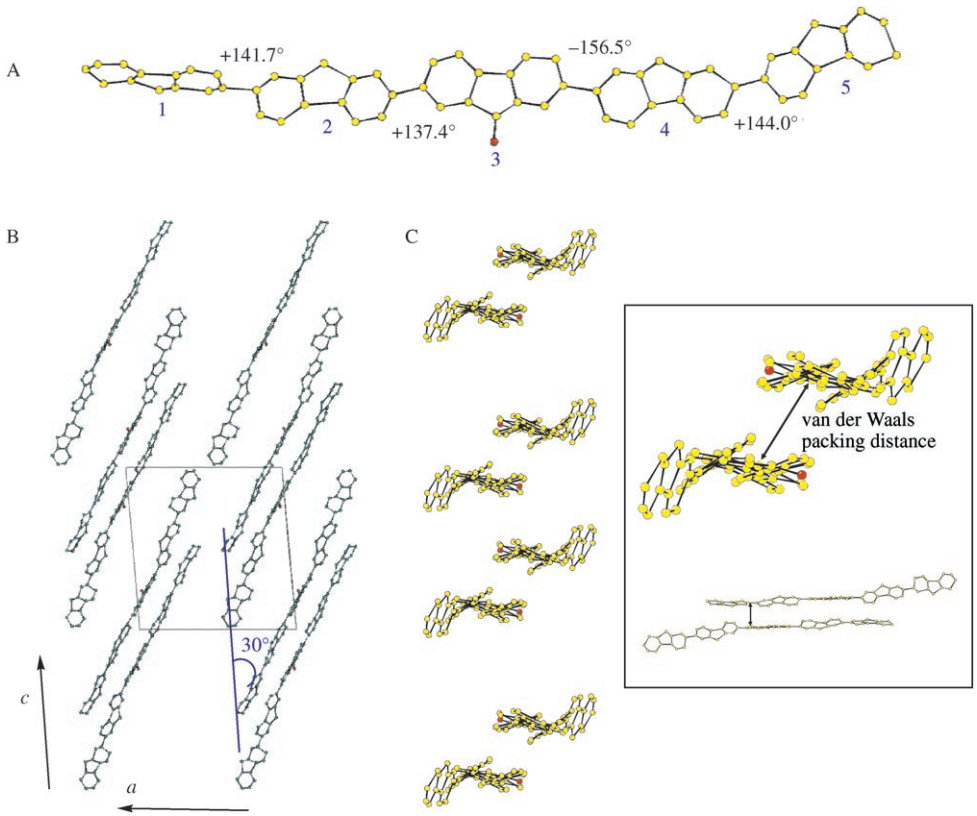

Figure 2. The single-crystal structure of the pentamer (**OF5K**). A) the conformation of the backbone without the aliphatic side-chains, the torsional angles between planes of adjacent fluorene/fluorenone units are indicated; B) the 3D packing projected on the *ac* plane. Note the stacking angle of 30° with regard to the *c* axis; C) the 3D packing structure projected along the molecular long axis. The molecules are packed in a distance in the range of van der Waals packing distance (3.8–4.0 Å, indicated by the arrow in the amplified Figure in frame).

remains unknown for the reasons explained above. The salient features of the packing of the oligomers are revealed in this projection. Rows of oligomers are inclined by 30° with regard to the *c* axis and the distance between adjacent rows is maintained by the space-filling aliphatic side groups. This feature is even better seen in the projection along the long axes of the oligomers shown in Figure 2C. Both projections indicate that although pairs of the helixlike molecules are packed in a distance in the range of van der Waals packing distance (3.8–4.0 Å, indicated by the arrow in Figure 2C), this packing is not an arrangement that can support excimer formation, as the planes of the fluorenes and fluorenones are neither parallel nor at close overlap. The dipolar coupling among fluorenone units gives rise to a packing characterized by a center of symmetry that relates adjacent oligomers crystallographically. Figure 2B also explains why the liquid crystal phase observed for these oligomers is, most probably, of the smectic type characterized by layers with the director axes of the molecules inclined to the layer plane.

Photophysical properties of OF*n*K

Steady-state UV-visible absorption and fluorescence: Steady-state UV-visible absorption and fluorescence spectra of **OF*n*K** dissolved in chloroform at the same fluorenyl unit concentration of 1.0×10^{-5} M are shown in Figure 3. The data extracted from these spectra and from spectra in a series of other solvents differing in polarity are collected in Table 1. In addition, the data of thin films (bulk state) of the oligomers are also given. The spectra of unsubstituted fluorenone are given in Figure 3 as well as a reference.

The **OF*n*K** exhibit a strong absorption peak related to the π–π* transition as observed in homo-oligofluorenes,[24] together with an additional broad absorption band at longer wavelengths (n–π* of the fluorenone unit; Figure 3 top). If the absorption spectra of **OF3K–OF7K** are normalized with regard to the intensity of the maximum of the absorption, the intensities of the fluorenone absorption bands decrease with the molecular size from **OF3K–OF7K**, because the amount of fluorenone component per molecule decreases with the chain length. The maximum of the absorption bands become red-shifted with increasing number (*n*) of fluorene units per molecule from **OF3K** ($\lambda_{max(abs)}=350$ nm, 3.54 eV) to **OF7K** ($\lambda_{max(abs)}=371$ nm, 3.34 eV). The molar extinction coefficients (ε) of **OF3K–OF7K** at the absorption peak of π–π* transition and n–π* transition in chloroform, as well as in a series of less polar solvents are shown in Table 2. The value of $\varepsilon_{\pi-\pi^*}$ increases linearly with increasing of chain length from **OF3K** to **OF7K**. The increment is ap-

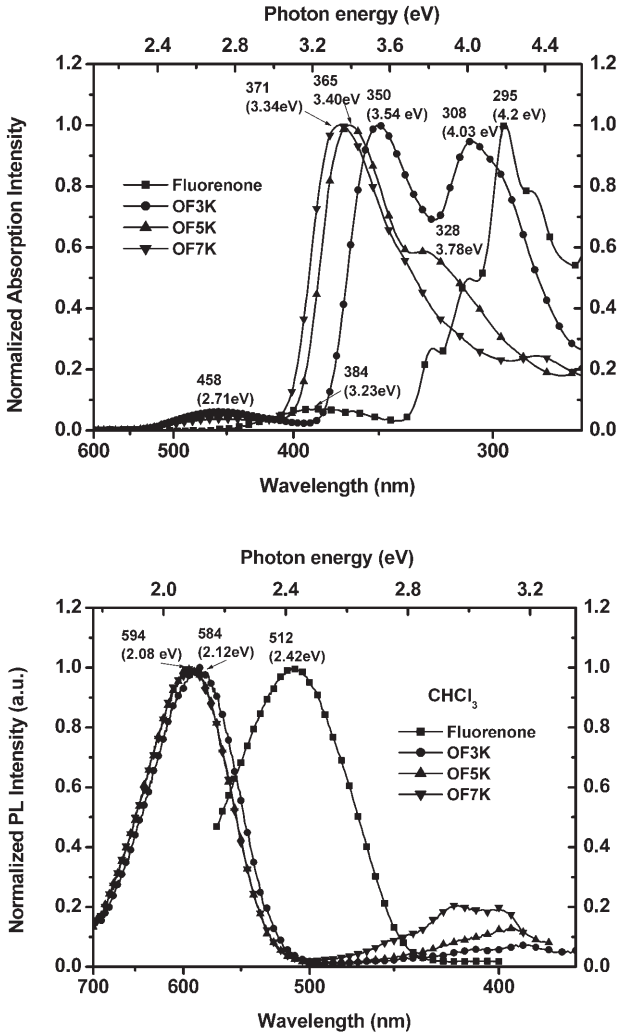

Figure 3. Steady-state UV-visible absorption (top) and fluorescence (bottom) spectra of fluorenone, **OF3K**, **OF5K**, and **OF7K** measured in chloroform (fluorene unit concentration $=1\times10^{-5}$ M) at room temperature.

Table 1. A summary of UV-visible absorption ($\lambda_{max(abs)}$) and fluorescence ($\lambda_{max(emi)}$) data for **OF3K**–**OF7K** in various solvents and as solid film on a quartz plate.

Solvent	**OF3K**		**OF5K**		**OF7K**	
	$\lambda_{max(abs)}$ [nm(eV)]	$\lambda_{max(emi)}$ [nm(eV)]	$\lambda_{max(abs)}$ [nm(eV)]	$\lambda_{max(emi)}$ [nm(eV)]	$\lambda_{max(abs)}$ [nm(eV)]	$\lambda_{max(emi)}$ [nm(eV)]
$CHCl_3$	350 (3.54)	584 (2.12)	366 (3.39)	594 (2.09)	371 (3.34)	596 (2.08)
toluene	349 (3.55)	532 (2.33)	365 (3.40)	535 (2.32)	371 (3.34)	535 (2.32)
2-MeTHF	348 (3.56)	532 (2.33)	364 (3.41)	537 (2.31)	370 (3.35)	536 (2.31)
methylcyclohexane	346 (3.58)	507 (2.45)	362 (3.43)	512 (2.42)	368 (3.37)	512 (2.42)
film	348 (3.56)	543 (2.28)	365 (3.40)	541 (2.29)	370 (3.35)	548 (2.26)

Table 2. Molar extinction coefficients (ε_{max}) at the absorption peak of π–π* transition and n–π* transition from various solutions.

	$\varepsilon_{\pi-\pi^*}$ [10^{-2} L mol^{-1} cm^{-1}]				$\varepsilon_{n-\pi^*}$ [10^{-2} L mol^{-1} cm^{-1}]			
	$CHCl_3$	toluene	2-MeTHF	MeCy	$CHCl_3$	toluene	2-MeTHF	MeCy
OF3K	638	632	675	661	39	42	45	42
OF5K	1329	1318	1404	1360	65	73	76	80
OF7K	2026	2016	2128	2130	76	85	94	90

proximately 34700 L mol^{-1} cm^{-1} per two fluorenyl units. In contrast with $\varepsilon_{\pi-\pi^*}$, the magnitude of $\varepsilon_{n-\pi^*}$ does not show an additivity rule. However, we note that the magnitude of $\varepsilon_{n-\pi^*}$ is still chain-length dependent; for example, going from **OF3K** to **OF7K** in chloroform is associated with ε going from 3900 to 7600 L mol^{-1} cm^{-1}. With all caution one could postulate that the $\varepsilon_{n-\pi^*}$ will saturate at further increase of n very soon. Zojer et al. predicted in a recent paper[22a] that $\varepsilon_{n-\pi^*}$ should not be dependent on n, but we cannot support this from our data. It is worth mentioning that Zojer et al. based their calculations on a molecular geometry of the ground state, which is also contradicted by our X-ray result (see above). In particular, the presence of the fluorenone group creates a helix reversal defect in the ground state that should be considered in further theoretical work aiming for detailed understanding of spectral features.

The fluorescence spectra of the same compounds in chloroform are shown in Figure 3 (bottom). The wavelength of the exciting light was fixed at the absorption maxima. A very strong unstructured yellow-green emission band accompanied by a weak blue emission was observed for **OF3K**–**OF7K**. The very weak blue emission with a well-resolved vibronic structure can be assigned to the 0–0, 0–1, and 0–2 excited singlet to ground state transitions.[2b,29] The emission band at lower energies is very similar to the "green" emission band observed in the photoluminescence and electroluminescence spectra of polyfluorenes. The maxima of the emission bands are red-shifted with increasing number (n) of fluorene units per molecule from **OF3K** ($\lambda_{max(emi)}=$ 584 nm, 2.12 eV) to **OF7K** ($\lambda_{max(emi)}=$596 nm, 2.08 eV). For fluorenone monomer (**OF1K**), the emission maximum occurs at 512 nm (2.42 eV).

The UV-visible absorption spectra of thin films of the compound **OF3K**–**OF7K** on quartz substrates are practically identical to those obtained from solutions except for a slight blue-shift, as listed in Table 1. However, their PL spectra in thin films are much more blue-shifted than those obtained from solutions of the oligomers in chloroform (540 nm vs 580–590 nm; see Figure 6 in the Supporting Information).

It is known that the energy level of the photoexcited state of chromophores containing both electron-donating and -withdrawing groups can be affected by solvation.[30] Both the peak position and the shape of the fluorescence spectra can be influenced by solvation. This is also found for the set of oligomers **OF*n*K**. For example, the normalized fluorescence spectra of **OF5K** in methylcyclohexane (MeCy), toluene, 2-methyltetrahydro-

furan (2-MeTHF), and chloroform are shown in Figure 4. The relevant data are listed in Table 1 (see also Figure 7 in the Supporting Information for **OF3K** and **OF7K**). The molar extinction coefficients ε of **OF3K**–**OF7K** for the absorption peaks of the π–π* and n–π* transitions show little dependence on solvent polarity (Table 2). The wavelength of the absorption maximum is slightly red-shifted with increasing solvent polarity. This indicates a positive solvatochromic response.[31] For example, in the case of **OF5K** we find a maximum solvatochromic shift of only 0.04 eV going from chloroform to MeCy as solvent. Similar behavior has been observed for donor–acceptor-substituted terthiophenes,[32] donor–acceptor oligomer 3,6-[bis(4-phenyl-2-quinolyl)]-9-methylcarbazole, and 3,7-[bis(4-phenyl-2-quinolyl)]-10-methylphenothiazine,[33] in which the same trend was rationalized as a consequence of an intramolecular charge transfer.

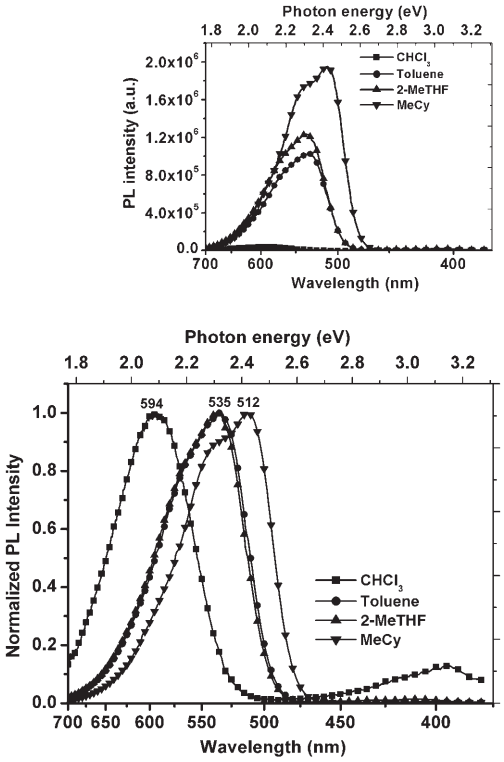

Figure 4. The fluorescence spectra of **OF5K** in solvents of different polarity (concentration: 1×10^{-5} M fluorene units, $\lambda_{exc}=365$ nm, inset shows the non-normalized fluorescence spectra).

The fluorescence spectra of **OF*n*K** are very sensitive to the polarity of the solvent. For example, the wavelength of the emission maximum of the fluorescence spectra of **OF5K** (1×10^{-6} M) shifts from 512 to 594 nm when going from MeCy as the least polar to chloroform as the most polar solvent (see Table 1). Consequently the Stokes shift increases with increasing polarity of the solvent. This indicates that the dipole moment of the photoexcited state is larger than that of the ground state.[34] It is also worth mentioning that the vibronic substructure of the emission becomes washed out as the polarity of the solvent increases. This effect is clearly seen in Figure 4 and it goes along with the observation that the full width at half-maximum (fwhm) of the emission for all oligomers increases from 82 (in MeCy, toluene, 2-MeTHF) to 100 nm (in chloroform). This results from local and time-dependence variations of the solvent environment of the chromophores.[34] The literature associates such phenomena with intramolecular charge transfer occurring within the excited molecule.[35]

The fluorescence intensities decrease going from nonpolar solvents to polar solvents (see the inset in Figure 4). As the energy of the excited state is lowered by solvation in polar solvents, the radiationless transition to the ground state generally become faster; at the same time the corresponding radiative transition, which depends on the third power of the frequency, will become slower. This line of thought gives a general rational explanation for the quenching action of polar solvents only if the excited state is more polar than the ground state.

Time-resolved fluorescence (TRF): To further understand the photophysics of **OF*n*K**, time-resolved fluorescence measurements were conducted by using a streak camera and gated detection technique at room temperature and at 77 K.

The fast time-resolved fluorescence spectra of **OF5K** as thin film and in solution are shown in Figure 5. A broad green emission band with maximum approximately at 2.30 eV (540 nm) was detected both in the mixed solvent toluene/MeCy and in the bulk at room temperature. This emission band matches exactly the previously reported "green" PL and EL band in blue-emitting polyfluorenes.[2] The strong "green" emission is accompanied by a weak blue emission when **OF5K** was excited at 370 nm in 2-MeTHF (Figure 5 bottom). The blue emission grows weaker at 77 K. The shape of the "green" emission of **OF5K** shows little dependence on the wavelength of the exciting light as demonstrated by Figure 5 (bottom) for 430 and 370 nm wavelengths of excitation.

At 77 K, the green emission band with well-resolved structure with peaks at approximately (2.25 eV) 550 nm and (2.10 eV) 590 nm was observed in both solution and film of **OF5K** (Figure 5). The shape of the spectra is very similar to the fluorescence spectra of the pentamer of **PF2/6** (**OF5**)[24] with a similar vibronic splitting of about 160 meV, indicating that that the green emission band does not originate from the formation of an excimer species. Similar behaviour was also observed for **OF3K** (see Figure 8 in the Supporting Information).

The **OF*n*K** may be regarded as models for polyfluorenes that have a certain fraction of fluorenone groups incorporated. On photoexcitation rapid energy transfer takes place from higher energy sites (fluorene segments) to lower energy sites (fluorenone units) prior to the radiative decay of the excited species.

The weak blue emission band in **OF5K** showed a monoexponential decay with lifetime of 573 ps (see Figure 9 in the Supporting Information), which is very similar to the

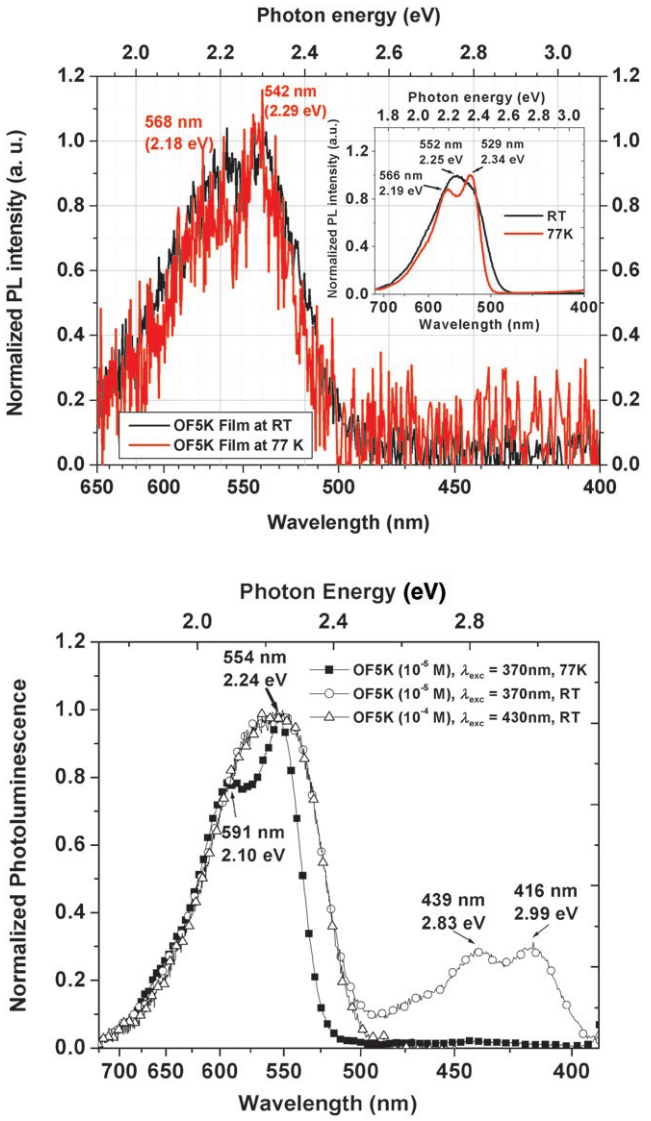

Figure 5. Top: The fluorescence spectra of the **OF5K** as thin film at both RT and 77 K (insert shows the fluorescence spectra of **OF5K** in dilute toluene/methylcyclohexane at two temperatures). Bottom: the fluorescence spectra of **OF5K** in 2-MeTHF solution at both RT and 77 K (excited at 430 and 370 nm, respectively).

decay of pure **OF5** (560 ps), suggesting that the blue emission band arises from the fluorenyl segments. This observation goes along with other phenomena already discussed in this work, in particular the strong distortion of the oligomers near the central fluorenone group. This topological defect seems to nearly isolate the two halves of the molecule from each other. This also explains the magnitude of the lifetime of the blue fluorescence in **OF5K**, which is bit longer that in **OF5**. The decay of the green emission is much slower (see Figure 10 in the Supporting Information). The lifetime can not be obtained from streak camera techniques; instead long-time-range-delayed fluorescence measurements were performed.

The delayed fluorescence (DF) spectra of **OF5K** (10^{-6} M) at 77 K in 2-MeTHF were evaluated to give the data shown in Figure 6. To verify the difference between absorption bands, namely, n→π* and π→π* transitions, **OF5K** was excited both at 365 and 453 nm.

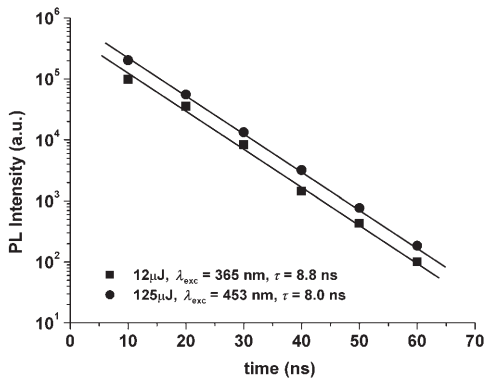

Figure 6. The dependence of DF intensity upon time ($t > 10$ ns) for **OF5K** (at 10^{-6} M) probed at 543 nm and 77 K in 2-MeTHF.

The frozen solution of **OF5K** in 2-MeTHF at 77 K (Figure 6) showed a monoexponential decay behaviour. The fluorescence lifetime is approximately 8 ns at both excitation conditions, which is much longer than that found for the blue emission band. Similar decay behaviour and lifetime (8.3 ns) were also observed for **OF3K** in the frozen matrix of 2-MeTHF at 77 K.

The dependence of continuous-wave (CW) fluorescence, prompt fluorescence, and delayed fluorescence intensity upon laser excitation intensity for **OF5K** in a dilute frozen solution at 77 K is shown Figure 7. The delayed emission

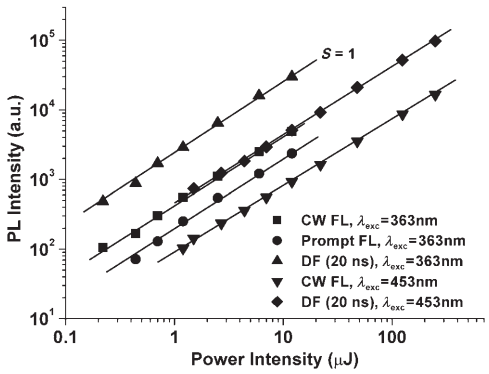

Figure 7. The dependence of CW, prompt, and DF intensity of **OF5K** (10^{-6} M) on laser excitation intensity at 77 K in 2-MeTHF probed at 546 nm (excited at 365 or 453 nm).

was recorded with a time delay of 20 ns after excitation at 363 and 453 nm. The CW, prompt, and delayed fluorescence intensity vary approximately linearly with laser excitation intensity probed at 546 nm, indicating that the excited species do not undergo further changes besides the return to the ground state.

To test possible concentration effects solutions of **OF5K** in 2-MeTHF were investigated with variation of the concentration between 10^{-6} and 10^{-3} M. The relevant CW fluorescence spectra observed at room temperature are shown in Figure 8 and the time dependence of the intensity probed at

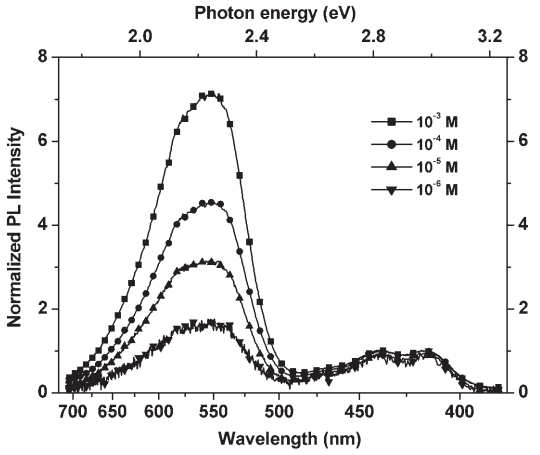

Figure 8. The fluorescence spectra of **OF5K** (normalized at 412 nm) in 2-MeTHF solutions with different concentrations at RT (excited at 365 nm), laser power: 100 μJ.

537 nm is depicted in Figure 9. When the CW spectra are normalized for the blue emission at 414 nm, the intensity of the green emission band at approximately 550 nm increases

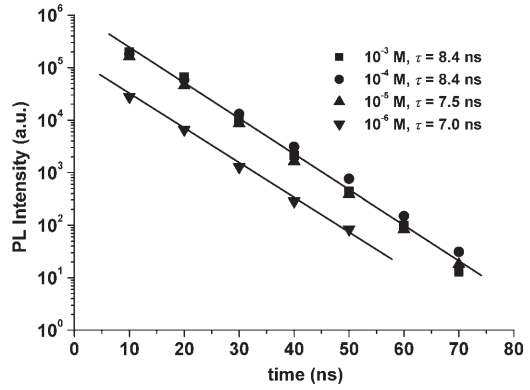

Figure 9. Dependence of fluorescence intensity of **OF5K** probed at 537 nm upon time for $t > 10$ ns in 2-MeTHF at different concentrations at RT (excited at 365 nm), laser power: 5 μJ.

by a factor of about six when the concentration of the fluorophore increases by three orders of magnitude from 10^{-6} to 10^{-3} M. The decay kinetics are not affected within the limits of error of the measurement and are strictly monoexponential. The concentration-independent shape of the CW spectra together with the decay kinetics points towards the presence of a single emitter. If the aggregates or clusters play a role, then the decay kinetics should become multiexponential[9e,36] and the fluorescence spectra should show different structure as the concentration changes by orders of magnitude. The weak dependence of the (normalized) fluorescence intensity on concentration in the green region of the spectrum can be explained by enhanced intermolecular quenching of the blue fluorescence upon increasing concentration,[37] which goes along with the observation that the green emission is only seen in the solid state of **OF5K**. The same dominance of the green emission has also been seen for fluorenone-group-containing polyfluorenes.[16d]

The observed lifetimes of the green emission in the **OF*n*K** are similar to those previously reported for 9-fluorenone,[38] and poly-(9,9-dihexylfluorene-*co*-fluorenone)s.[20] This is in good agreement with other recent reports[16a,c,d] that the green emission in **OF*n*K** originates from the fluorenone units situated on individual chains, but not from formation of excimers.

Energy level analysis: Cyclic voltammetry was used to determine the energy levels of the highest occupied molecular orbital (HOMO) and lowest unoccupied molecular orbital (LUMO) of **OF*n*K**. In all cases, multiple reversible oxidation waves and one reduction wave were observed. The cyclic voltammetry curves are shown in Figure 10 and the

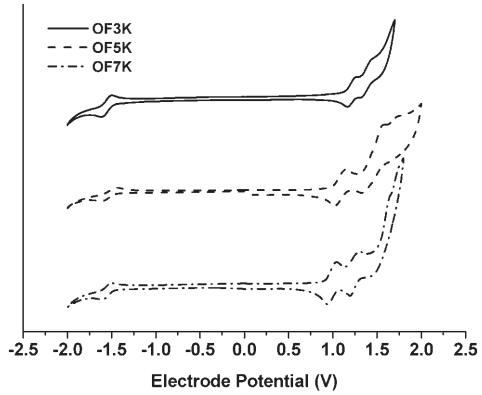

Figure 10. Cyclic voltammetry curves of **OF*n*K** probed in dichloromethane (see Experimental Section).

data retrieved from them are given in Table 3. With the extension of the chain length, the half wave potentials ($E_{1/2}$) for the equivalent oxidation waves displayed a negative shift. For example, for **OF3K**, two reversible oxidation waves with $E^1_{1/2}$ and $E^2_{1/2}$ at 1.20 and 1.38 V, respectively, were observed. They are assigned to the successive genera-

Table 3. Cyclic voltammetric data for **OF3K**–**OF7K**.[a,b]

	$E^1_{1/2}$(Ox) [V]	$E^2_{1/2}$(Ox) [V]	$E^2_{1/2}-E^1_{1/2}$[c] [V]	$E^1_{1/2}$(Red) [V]	I_p [eV]	E_a [eV]	ΔE [eV]
OF3K	1.20	1.38	0.18	−1.54	5.73	3.13	2.60
OF5K	1.08	1.37	0.29	−1.52	5.61	3.14	2.47
OF7K	1.02	1.26	0.24	−1.53	5.52	3.13	2.39

[a] Scan rate: 100 mv s^{-1}, for Fc$^+$/Fc, $E_{1/2} = 0.232$ V was used as standard. Concentration of substrate was 5×10^{-4} M in 0.1 M Bu_4NPF_6 in CH_2Cl_2. [b] Ionization potential (I_p) and electron affinity (E_a) are given relative to the vacuum level. [c] Oxidation potentials.

tion of the radical monocation and dication of the compound. The pentamer **OF5K** gave two reversible oxidation waves with $E^1_{1/2}$ and $E^2_{1/2}$ at 1.08 and 1.37 V, respectively. However, all of the compounds **OF*n*K** gave only one reduction wave with $E^1_{1/2}$ around −1.53 V that did not show any chain-length dependence.

The redox potentials were internally calibrated by adding ferrocene (Fc) during the measurements and in the case of using $AgNO_3$/Ag as reference electrode the $E_{1/2}(Fc^+/Fc)$ was 0.232 V. Thus, ionization potential (I_p in eV, HOMO) and electron affinity (E_a in eV, LUMO) relative to the vacuum level can be derived from Equations (1) and (2), respectively, in which E_{ox} and E_{red} are the onset potentials for oxidation and reduction relative to $AgNO_3$/Ag reference electrode.[39]

$$I_p = (E_{ox} + 4.4 + 0.435 - 0.232) \quad (1)$$

$$E_a = (E_{red} + 4.4 + 0.435 - 0.232) \quad (2)$$

The value of I_p decreases with extension of the chain length from 5.73 eV for **OF3K** to 5.52 eV for **OF7K**, whereas E_a remains unchanged, resulting in a convergent behavior of the HOMO–LUMO gap (ΔE is calculated from $\Delta E = I_p - E_a$). This indicates that E_a is strongly confined to the fluorenone unit. The trend of the values of I_p and E_a with chain length is consistent with results of quantum-chemical calculations of the energies of HOMO and LUMO of **OF*n*K.**[40]

With these data in hand, we can combine our experimental results with quantum-chemical calculations reported by Zojer and co-workers[22a] to gain a better understanding of the photophysical properties of **OF*n*K**. These authors have calculated the transition energies and oscillator strengths for the relevant excited states of the model molecule **OF5K** starting from the ground-state equilibrium geometry. For **OF5K**, the S_0–S_1 transition corresponds to an optically forbidden transition and possesses n→π* character. Such low-lying n–π* states are common in aromatic ketones. The next excited state (S_2) is also only weakly optically allowed and the excitation to the S_2 state is associated with a significant charge redistribution in the fluorenone unit, thus the S_2 can be classified as a π–π* charge-transfer (CT) state. The first state with high oscillator strength in **OF5K** is the third singlet excited state S_3. The energy level diagram show in Figure 11 summarizes these results.

The absorption is very weak in the low-energy range of the absorption spectra as is experimentally seen in Figure 3, because the low-lying states in fluorenone-containing chains (S_1 and S_2 in Figure 11) possess very low oscillator strength. They can hardly be observed in the absorption spectra of materials with low fluorenone concentration. This is also consistent with the lack of absorption in the low energy region observed in photodegradation experiments on polyfluorenes.[7,22a,20] Consequently, the products of photo- and/or electrooxidation will become accessible through absorption spectroscopy only in strongly degraded materials.[16a,29]

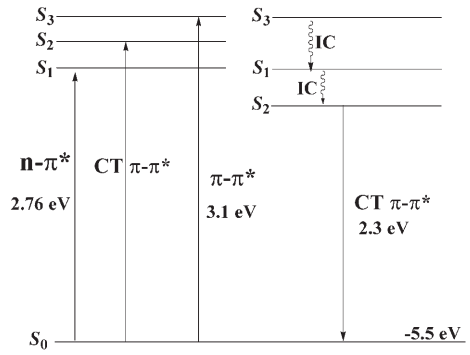

Figure 11. Energy level diagram for **OF5K** derived from data of this work from cyclic voltammetry and spectroscopy in combination with quantum-chemical calculations.[21a]

We now discuss why a strong green emission can be observed in **OF*n*K**. The energy-level diagram for **OF5K** indicate that relaxation phenomena take place from the lowest lying excited state as revealed by Zojer et al.[22a] Such geometric relaxation in the excited state leads to a reversal in the ordering of the two lowest excited states, with the first excited state becoming the CT π–π* excitation as indicated in Figure 12. The vertical transition energy from the first relaxed singlet excited state to the ground state for **OF5K** is very close to the experimentally observed yellow-green emission (2.1–2.4 eV). In addition, the small, but nonvanishing, oscillator strength associated with the CT π–π* excited state is in agreement with the experimental observations: 1) the fluorenone defect *is emissive*, but 2) the quantum efficiencies of fluorenone-containing materials are very low. In fact, the quantum efficiency of **OF5K** drops significantly with respect to the pure pentafluorene. Similarly, the fluorescence of the photooxidized films is also significantly decreased compared to pristine polyfluorenes.[29]

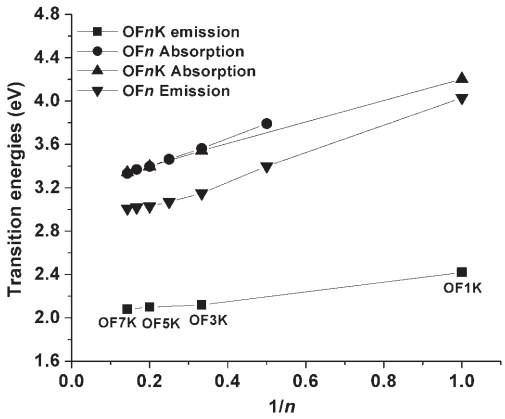

Figure 12. The dependence of transition energies on the reciprocal number of fluorene units (n) for **OF*n*** and **OF*n*K**.

Quantum-chemical calculations for the fluorenone monomer **OF1K**[22a] reveal that: 1) the energies of the n–π* states are almost identical in **OF1K** and **OF5K**, 2) the shift between the CT π–π* states of **OF1K** and the longer model

systems is relatively small (0.33 eV), and 3) the energy difference between the π–π* states in **OF1K** and **OF5K** is quite large (around 1.4 eV). The dependence of the excited state energies on the chain length for **OF5** and **OF5K** is shown in Figure 12, based on UV-visible absorption and fluorescence data.[24] Oligomers **OF*n*** display a linear dependence of the energy level of the S_1 on the inverse number of repeat units, as is common for the energies of π–π* excited states in conjugated organic materials.[39a] The energies of the S_3 (S_5 for $n=1$) states in the fluorenone-containing materials show a similar trend. This is consistent with the results from quantum-chemical calculations: the S_3 (π–π*) state is delocalized along the whole chain.[22a] In contrast, the energy of the S_1 state (n–π*) in **OF*n*K** is chain-length independent (Figure 3). As described above, the absorption maximum wavelength corresponding to S_3 (π–π*) (S_5 $n=1$) is red-shifted with the molecular length of **OF*n*K**, while the long-wave absorption maximum (S_1, n–π*) is almost constant from **OF3K** to **OF7K**. The two lowest lying excited states (S_1 (n–π*) and S_2 (CT π–π*)) in the fluorenone-containing materials are strongly localized to the immediate environment of the keto group.[22a] The localization is even more pronounced for the n–π* state. For the CT π–π* excited state, a nonvanishing electron-hole density is also distributed on the neighboring fluorene units, but it tapers off rapidly with increasing chain length. This indicates that at least the fluorene segments that are directly attached to the fluorenone unit affect, to a certain extent, the electronic structure of the S_2 state. For **OF*n*K**, the calculated energy of the S_2 (CT π–π*) state decreases by 0.31 eV when going from **OF1K** to the **OF3K** and then remains constant upon further increase of chain length.

As shown in Figure 3, the ratio of blue over green emission intensity increases with increasing chain length. This relates to the increasing fraction of fluorene units in the higher oligomers. In addition, the blue emission band becomes also red-shifted as the molecular length increases due to the delocalized π–π* state. Thus the nature of the green and blue emissions from **OF*n*K** and their chain length dependence can be reasonably accounted for combining theory and experiment.

PFs/OFnK blends: The above discussions demonstrated that efficient funneling of excitation energy takes place from the high-energy states on the fluorene segments to low-energy sites on the fluorenone units by hopping along a single oligomer or polymer chain. When the energy becomes trapped on the fluorenone site a yellow-green emission will be the consequence. In addition, the green emission may also arise from Förster-type interchain excitation energy transfer from fluorene segments of one chain to fluorenone units of an adjacent chain. To clarify this question in an unambiguous way the intermolecular energy transfer was investigated by using a model system consisting of ketone free polyfluorenes doped by small amounts of **OF*n*K**. The **OF*n*K** are completely miscible with the homopolymer both in solution and in the solid state.

The UV-visible absorption and steady state fluorescence spectra (excited at 383 nm) of thin films **PF2/6** doped with different concentrations of **OF3K** are shown in Figure 13. The spectra were taken at room temperature. The absorption spectra of the blends doped with 0.1, 0.3, 1, 3, 10 wt% **OF3K** are almost the same and resemble that of pure **PF2/6** independent of the concentration of the dopant. Comparing with the absorption spectra of **OF3K** as film (see Figure 6 in the Supporting Information), the n→π* band of the keto-group-containing moiety with a broad long-wave absorption maximum and a shoulder was not resolved in the blend system. This is, however, not surprising as the concentration of keto groups is relatively low in our doping experiments, which makes them difficult to detect by absorption measurements. Further, the typical spectral features of polyfluorenes are observed in all of the emission spectra (Figure 13 bottom) namely a maximum at 2.94 eV (422 nm) with a vibronic shoulder at 2.80 eV (443 nm). Upon increasing the concentration of the dopant **OF3K** from 0.3% to 10%, an additional green emission band with maximum at 2.35 eV

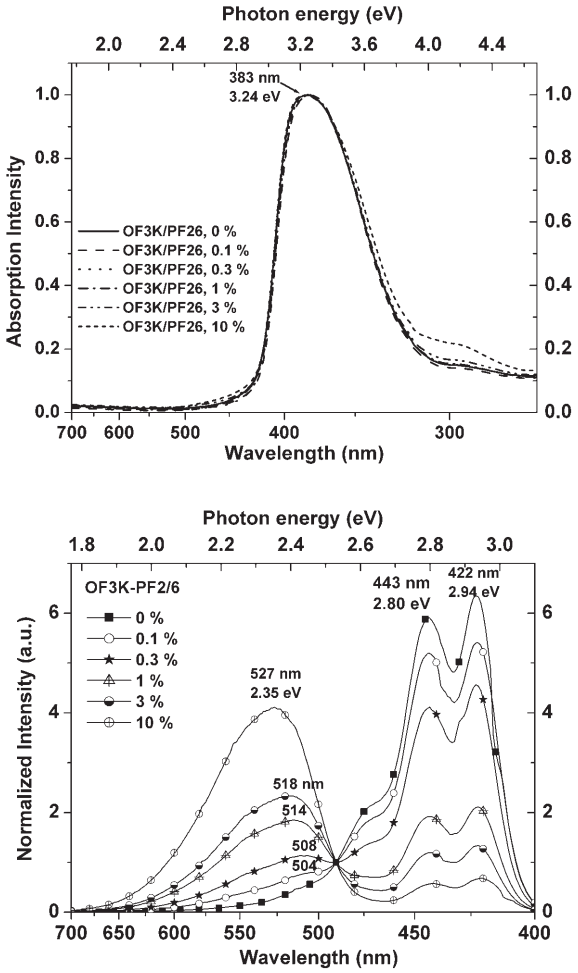

Figure 13. The UV-visible absorption (top) and steady-state fluorescence spectra, normalized at 490 nm (bottom) of **PF2/6** doped with different concentrations of **OF3K** ($\lambda_{exc}=383$ nm), measured at room temperature.

(527 nm) similar to that observed for thin films of **OF3K** can be detected. The emission spectra were normalized at 490 nm, to clearer see that the green emission intensity increases, while the blue emission intensity decreases with increasing of concentration of the dopant. When using **OF5K** instead of **OF3K** the same phenomena were seen (see Figure 11 in Supporting Information) The ratio of green emission intensity to the blue emission intensity measured at peak maximum in the **OF3K-PF2/6** blend increases with the concentration of dopant, that is, the concentration of keto groups in the system as is recorded in Table 4.

Table 4. A compilation of the ratio of green to blue emission intensity, the lifetimes τ of blue emission, the energy-transfer rate constants (k_T), and energy-transfer efficiencies (φ_T) obtained for **OF3K-PF2/6** and **OF5K-PF2/6** blends at various concentrations of **OF*n*K**.

c[a]	Ratio[b]			τ_{blue} [ps][c]			k_T[d] [ns^{-1}]			φ_T[e]		
	OF3K RT	**OF5K** RT	**OF5K** 77 K	**OF3K** RT	**OF5K** RT	**OF5K** 77 K	**OF3K** RT	**OF5K** RT	**OF5K** 77 K	**OF3K** RT	**OF5K** RT	**OF5K** 77 K
0	–	–	–	273	274	395	0	0	0	0	0	0
0.1	0.1	–	–	255	257	376	0.26	0.24	0.13	0.07	0.06	0.05
0.3	0.3	0.2	–	186	201	254	1.72	1.33	1.41	0.32	0.27	0.35
1	0.9	0.4	0.15	84	112	237	8.24	5.28	1.69	0.69	0.59	0.40
3	1.7	1.2	0.5	52	63	117	15.57	12.22	6.02	0.81	0.77	0.70
10	6.2	4.4	1.8	33	36	58	26.64	24.13	14.71	0.88	0.87	0.85

[a] Concentration of dopant wt%. [b] The values listed are the ratios of green emission at maximum intensity/blue emission at maximum intensity. [c] The values listed are lifetimes of the blue emission. [d] The energy-transfer rate constant (k_T). [e] Energy-transfer efficiency (φ_T).

The time-resolved decay of the fluorescence for **OF3K-PF2/6** blends probed at 422 nm at various doping concentrations at room temperature is shown in Figure 14 (for **OF5K-PF2/6**, see Figure 12 in the Supporting Information). A monoexponential decay is observed for the blue emission in the cases of low doping concentration. The decay becomes multiexponential at concentrations equal or larger than 3% and the lifetime of the blue emission of the **OF*n*K-PF2/6** blends decreases with the doping concentration. The precise data are listed in Table 4. Here, only the linear part of the decay curves for 3 and 10% of dopant was analyzed. The lifetime decreases from 273 to 33 ps when the doping concentration increases from 0 to 10 wt%, indicating a systematical increase of the quenching rate with increasing concentration of **OF*n*K**. In addition, the energy-transfer process is thermally activated. The lifetime of the blue emission from **OF5K-PF2/6** blend system at 77 K is higher compared to that at RT at the same doping concentration (Table 4), indicating that the energy transfer from **PF2/6** to **OF*n*K** is faster at higher temperature.

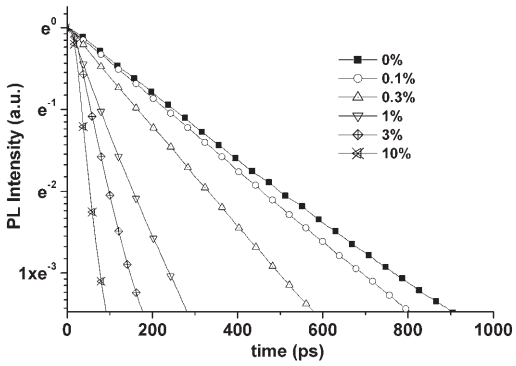

Figure 14. The decay of fluorescence of **OF3K-PF2/6** blends probed at 422 nm (λ_{exc} = 383 nm).

Although the excitation transport (or energy migration) can also take place within **OF*n*K** itself from the fluorene units to the central fluorenone group, the main energy transfer discussed here occurs from **PF2/6** to **OF*n*K** in the blends. The absorption spectra of **OF*n*K** and the fluorescence spectra of **PF2/6** in form of their films overlap in the range of 400–550 nm (see Figure 13 in the Supporting Information); hence, radiative transfer is possible by the absorption of a photon that is emitted by **PF2/6** donor by a molecule of **OF*n*K** as an acceptor. This would be a trivial situation.

In a classical molecular crystal the rate-limiting process for excitation quenching is the exciton migration within the host matrix. In a noncrystalline glassy medium composed of a conjugated polymer this is a dispersive process, because the energy levels associated with the subunits of the polymer are distributed in energy. This gives rise to energetic relaxation of the exciton and, concomitantly, to a reduction of the exciton mobility.[41] For Förster-type energy transfer,[42] dipole–dipole interactions control the individual transfer steps from an excited donor to an acceptor. If the fluorescence decay of the donor following pulsed excitation is a single exponential, the measurement of the decay time in the presence (τ_D) and absence (τ_D^0) of transfer allows us to determine the transfer rate constant k_T and the transfer efficiency φ_T, by using Equations (3) and (4):[34b]

$$k_T = \frac{1}{\tau_D} - \frac{1}{\tau_D^0} \quad (3)$$

$$\Phi_T = 1 - \frac{\tau_D}{\tau_D^0} \quad (4)$$

As Table 4 and Figure 15 show, the transfer rate constant (k_T) and the transfer efficiency (φ_T) increase with increasing doping concentration in all of the cases; further, k_T and φ_T increase faster for the **OF5K-PF2/6** blends at room temperature than at 77 K, and the energy-transfer efficiency becomes almost saturated as the **OF*n*K** concentration approaches 3 wt%.

Conclusion

Oligofluorenes with a keto defect in the center (**OF*n*K**) were prepared and were used as model compounds to un-

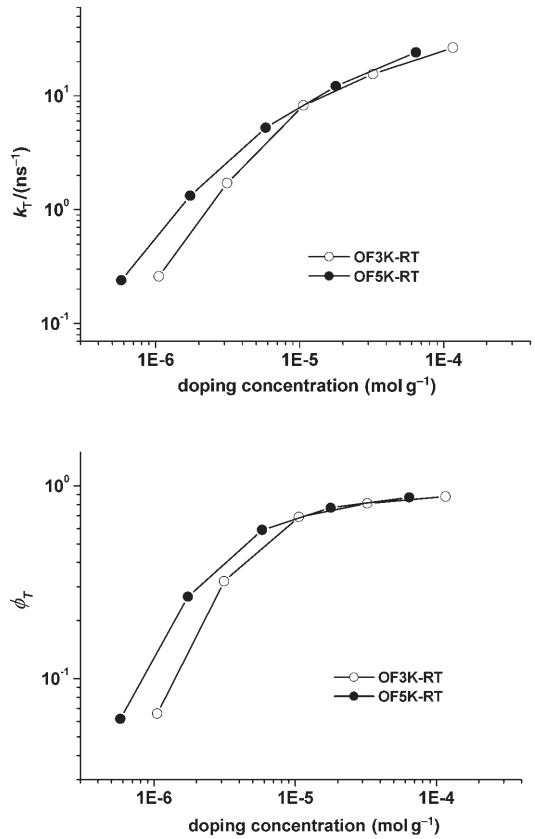

Figure 15. The dependence of k_T and φ_T on the doping concentration for **OF3K**-**PF2/6** and **OF5K**-**PF2/6** blends.

derstand the origin of the low-energy emission band that occurs upon oxidation in the photo- and electroluminescence spectra of polyfluorenes. A smectic liquid crystalline phase was found to exist between the glass transition temperature and the liquid crystal to isotropic phase transition in **OF5K** and **OF7K**. Crystals of **OF5K** could be obtained and analyzed for the three-dimensional packing of the molecules. Despite of inherent disorder caused by the side groups, the diffraction data could be analyzed to give the conformational angles in the backbone. The repeat units are arranged in a helical conformation with helix reversal at the central fluorenone unit. This results in an overall nonplanar shape that prevents close packing of adjacent chains to a distance and geometry that would be prerequisite for formation of excimer configurations. The photophysical properties of **OF*n*K** were studied in dilute solution and as thin films. The steady-state UV-visible spectra disclose a strong absorption of π–π* character accompanied by a weak long-wavelength absorption assigned to an n–π* transition. The fluorescence spectra reveal a strong broad green emission band. This green emission is identical to the low-energy emission of photo- or electrooxidized PFs.

The strong green emission of **OF*n*K** suggests that rapid energy transfer takes place from higher energy sites of the fluorene segments to lower energy sites of the fluorenone units prior to the radiative decay of the excited species. Monoexponential decay behaviour was observed. The lifetime of the green band is about 8 ns for **OF3K** and **OF5K**. Independence of the monoexponential decay behaviour on concentration rules out that the green emission band originates from aggregates, neither in the ground nor the excited state.

The position of low-energy absorption and the green emission is independent of the chain-length of **OF*n*K**. This comes from the situation that the n–π* state and CT π–π* are localized dominantly on the central fluorenone unit of **OF*n*K**.

Energy transfer was investigated using a model system of a polyfluorene doped by **OF*n*K**. Förster-type energy transfer takes place from **PF2/6** to **OF*n*K**, and the energy-transfer efficiency increases with increasing doping concentration. The green emission in the photochemically or thermally degraded polyfluorenes can therefore be ascribed to 1) efficient funneling of excitation energy from the high-energy fluorene segments to the low-energy fluorenone defects by hopping of excitations along a single polymer chain until they are trapped on the fluorenone defects on that chain and 2) interchain Förster-type energy-transfer processes.

Experimental Section

The electrochemical measurements of **OF3K**–**OF7K** (5.0×10^{-4} M in dry dichloromethane) were performed in a standard three-electrode cell, a platinum wire sealed in insulated rubber as working electrode, a $AgNO_3$/Ag nonaqueous electrode as reference electrode, and a platinum wire as counter electrode. Tetrabutylammonium hexafluorophosphorate ($TBAPF_6$, 0.1 M) was used as supporting electrolyte. The electrochemical potentials were calibrated by an internal reference couple ferrocene/ferrocenium (Fc/Fc^+) in each measurements and in all case $E_{1/2}$ (Fc/Fc^+) = 0.232 V.

Other experimental details are available in the Supporting Information.

Acknowledgements

This work was supported by a project of the EU in the 5FRP (contract number: HPRN-CT-2000–0003). The authors would like to thank P. Keivanidis, F. Laquai, and J. Wu for fruitful discussion.

[1] a) G. Grem, G. Leditzky, B. Ullrich, G. Leising, *Adv. Mater.* **1992**, *4*, 36–37; b) Y. Yang, Q. Pei, A. J. Heeger, *J. Appl. Phys.* **1996**, *79*, 934–939; c) Q. Pei, Y. Yang, *J. Am. Chem. Soc.* **1996**, *118*, 7416–7417; d) A. W. Grice, D. D. C. Bradley, M. T. Bernius, M. Inbasekaran, W. W. Wu, E. P. Woo, *Appl. Phys. Lett.* **1998**, *73*, 629–631; e) M. Berggren, O. Inganäs, G. Gustafsson, J. Rasmusson, M. R. Andersson, T. Hjertberg, O. Wennerström, *Nature* **1994**, *372*, 444–446; f) A. Hilberer, H.-J. Brouwer, B.-J. van der Scheer, J. Wildeman, G. Hadziioannou, *Macromolecules* **1995**, *28*, 4525–4529; g) F. Garten, A. Hilberer, F. Cacialli, E. Esselink, Y. van Dam, B. Schlatmann, R. H. Friend, T. M. Klapwijk, G. Hadziioannou, *Adv. Mater.* **1997**, *9*, 127–131; h) W.-L. Yu, J. Pei, Y. Cao, W. Huang, A. J. Heeger, *Chem. Commun.* **1999**, 1837–1838; i) W.-L. Yu, Y. Cao, J. Pei, W. Huang, A. J. Heeger, *Appl. Phys. Lett.* **1999**, *75*, 3270–3272.

[2] a) U. Scherf, E. J. W. List, *Adv. Mater.* **2002**, *14*, 477–487; b) D. Neher, *Macromol. Rapid Commun.* **2001**, *22*, 1365–1385.

[3] D. Sainova, T. Miteva, H. G. Nothofer, U. Scherf, I. Glowacki, J. Ulanski, H. Fujikawa, D. Neher, *Appl. Phys. Lett.* **2000**, *76*, 1810–1812.
[4] a) A. R. Buckley, M. D. Rahn, J. Hill, J. Cabanillas-Gonzalez, A. M. Fox, D. D. C. Bradley, *Chem. Phys. Lett.* **2001**, *339*, 331–336; b) D. F. O'Brien, C. Giebeler, R. B. Fletcher, A. J. Cadby, L. C. Palilis, D. G. Lidzey, P. A. Lane, D. D. Bradley, W. Blau, *Synth. Met.* **2001**, *116*, 379–383; c) X. Gong, J. C. Ostrowski, G. C. Bazan, D. Moses, A. J. Heeger, M. S. Liu, A. K-Y. Jen, *Adv. Mater.* **2003**, *15*, 45–49.
[5] J. R. Sheats, H. Antoniadis, M. Hueschen, W. Leonard, J. Miller, R. Moon, D. Roitman, A. Stocking, *Science* **1996**, *273*, 884–888.
[6] R. D. Scurlock, B. Wang, P. R. Ogilby, J. R. Sheats, R. J. Goitia, *J. Am. Chem. Soc.* **1995**, *117*, 10194–10202.
[7] V. N. Bliznyuk, S. A. Carter, J. C. Scott, G. Klärner, R. D. Miller, D. C. Miller, *Macromolecules* **1999**, *32*, 361–369.
[8] a) F. Uckert, Y. H. Tak, K. Müllen, H. Bässler, *Adv. Mater.* **2000**, *12*, 905–908; b) K. H. Weinfurtner, H. Fujikawa, S. Tokito, Y. Taga, *Appl. Phys. Lett.* **2000**, *76*, 2502–2504.
[9] a) U. Lemmer, S. Heun, R. F. Mahrt, U. Scherf, M. Hopmeier, U. Siegner, E. O. Göbel, K. Müllen, H. Bässler, *Chem. Phys. Lett.* **1995**, *240*, 373–378; b) V. Cimrová, U. Scherf, D. Neher, *Appl. Phys. Lett.* **1996**, *69*, 608–610; c) E. Conwell, *Trends Polym. Sci.* **1997**, *5*, 218–222; d) M. Grell, D. D. C. Bradley, G. Ungar, J. Hill, K. S. Whitehead, *Macromolecules* **1999**, *32*, 5810–5817; e) S. A. Jenekhe, J. A. Osaheni, *Science* **1994**, *265*, 765–768; f) W. L. Yu, J. Pei, W. Huang, A. J. Heeger, *Adv. Mater.* **2000**, *12*, 828–831; g) M. Kreyenschmidt, G. Klaerner, T. Fuhrer, J. Ashenhurst, S. Karg, W. D. Chen, V. Y. Lee, J. C. Scott, R. D. Miller, *Macromolecules* **1998**, *31*, 1099–1103; h) J. Teetsov, M. A. Fox, *J. Mater. Chem.* **1999**, *9*, 2117–2122.
[10] C. Ego, A. C. Grimsdale, F. Uckert, G. Yu, G. Srdanov, K. Müllen, *Adv. Mater.* **2002**, *14*, 809–811.
[11] T. Miteva, A. Meisel, W. Knoll, H. G. Nothofer, U. Scherf, D. C. Muller, K. Meerholz, A. Yasuda, D. Neher, *Adv. Mater.* **2001**, *13*, 565–570.
[12] a) G. Zeng, W.-L. Yu, S.-J. Chua, W. Huang, *Macromolecules* **2002**, *35*, 6907–6914; b) Y. He, S. Gong, R. Hattori, J. Kanicki, *Appl. Phys. Lett.* **1999**, *74*, 2265–2267; c) G. Klaerner, M. H. Davey, W. D. Chen, J. C. Scott, R. D. Miller, *Adv. Mater.* **1998**, *10*, 993–997; d) S. Xiao, M. Nguyen, X. Gong, Y. Cao, H. B. Wu, D. Moses, A. J. Heeger, *Adv. Funct. Mater.* **2003**, *13*, 25–29.
[13] S. Setayesh, A. C. Grimsdale, T. Weil, V. Enkelmann, K. Müllen, F. Meghdadi, E. J. W. List, G. Leising, *J. Am. Chem. Soc.* **2001**, *123*, 946–953.
[14] A. P. Kulkarni, S. A. Jenekhe, *Macromolecules* **2003**, *36*, 5285–5296.
[15] A. J. Campbell, D. D. C. Bradley, T. Virgili, D. G. Lidzey, H. Antoniadis, *Appl. Phys. Lett.* **2001**, *79*, 3872–3874.
[16] a) E. J. W. List, R. Güntner, P. Scandiucci de Freitas, U. Scherf, *Adv. Mater.* **2002**, *14*, 374–378; b) X. Gong, P. K. Iyer, D. Moses, G. Bazan, A. J. Heeger, S. S. Xiao, *Adv. Funct. Mater.* **2003**, *13*, 325–330; c) J. M. Lupton, M. R. Craig, E. W. Meijer, *Appl. Phys. Lett.* **2002**, *80*, 4489–4491; d) L. Romaner, A. Pogantsch, P. Scandiucci de Freitas, U. Scherf, M. Gaal, E. Zojer, E. L. W. List, *Adv. Funct. Mater.* **2003**, *13*, 597–601; e) D. Sainova, D. Neher, E. Dobruchowska, B. Luszczynska, I. Glowacki, J. Ulanski, H.-G. Nothofer, U. Scherf, *Chem. Phys. Lett.* **2003**, *371*, 15–22; f) M. Gaal, E. J. W. List, U. Scherf, *Macromolecules* **2003**, *36*, 4236–4237.
[17] H.-G. Nothofer, Ph.D. Thesis, Universität Potsdam (Germany), **2001**.
[18] a) S. Panozzo, J.-C. Vial, Y. Kervella, O. Stéphan, *J. Appl. Phys.* **2002**, *92*, 3495–3502; b) P. Scandiucci de Freitas, U. Scherf, M. Collon, E. Zojer, E. J. W. List, *e-Polym.* **2002**, 0009(1–7).
[19] J. I. Lee, G. Klärner, R. D. Miller, *Chem. Mater.* **1999**, *11*, 1083–1088.
[20] A. P. Kulkarni, X. Kong, S. A. Jenekhe, *J. Phys. Chem. B* **2004**, *108*, 8689–8701.
[21] a) E. J. W. List, G. Leising, N. Schulte, A. D. Schlüter, U. Scherf, W. Graupner, *Jpn. J. Appl. Phys. Part 2* **2000**, *39*, L760–L762; b) S. Tasch, E. J. W. List, C. Hochfilzer, G. Leising, P. Schlichting, U. Rohr, Y. Geerts, U. Scherf, K. Müllen, *Phys. Rev. B* **1997**, *56*, 4479–4483.
[22] a) E. Zojer, A. Pogantsch, E. Hennbebicq, D. Beljonne, J.-L. Brédas, P. Scandiucci de Freitas, U. Scherf, E. J. W. List, *J. Chem. Phys.* **2002**, *117*, 6794–6802; b) I. Franco, S. Tretiak, *Chem. Phys. Lett.* **2003**, *372*, 403–408.
[23] I. Prieto, J. Teetsov, M. A. Fox, D. A. Vanden Bout, A. J. Bard, *J. Phys. Chem. A* **2001**, *105*, 520–523.
[24] J. Jo, C. Chi, S. Höger, G. Wegner, D. Y. Yoon, *Chem. Eur. J.* **2004**, *10*, 2681–2688.
[25] a) T. Ishiyama, M. Murata, N. Miyaura, *J. Org. Chem.* **1995**, *60*, 7508–7510; b) M. W. Read, J. O. Escobedo, D. M. Willis, P. A. Beck, R. M. Strongin, *Org. Lett.* **2000**, *2*, 3201–3204; c) A. Giroux, Y. Han, P. Prasit, *Tetrahedron Lett.* **1997**, *38*, 3841–3844.
[26] P. Papadopoulos, G. Floudas, C. Chi, G. Wegner, *J. Chem. Phys.* **2004**, *120*, 2368–2374.
[27] a) C. Chi, Ph.D. Thesis, Johannes Gutenberg-University Mainz, **2004**; b) C. Chi, G. Lieser, V. Enkelmann, G. Wegner, unpublished results.
[28] a) G. Lieser, M. Oda, T. Miteva, A. Meisel, H. G. Nothofer, U. Scherf, D. Neher, *Macromolecules* **2000**, *33*, 4490–4495; b) M. Knaapila, B. P. Lyons, K. Kisko, J. P. Foreman, U. Vainio, M. Mihaylova, O. H. Seeck, L.-O. Pålsson, R. Serimaa, M. Torkkeli, A. P. Monkman, *J. Phys. Chem. B* **2003**, *107*, 12425–12430.
[29] S. Gamerith, C. Gadermaier, U. Scherf, E. J. W. List, *Phys. Status Solidi A* **2004**, *201*, 1132–1151.
[30] a) D. Oelkrug, A. S. Tompert, J. Gierschner, H.-J. Egelhaaf, M. Hanack, M. Hohloch, E. Steinhuber, *J. Phys. Chem. B* **1998**, *102*, 1902–1907; b) B. Strehmel, A. M. Sarker, J. H. Malpert, V. Strehmel, H. Seifert, D. C. Neckers, *J. Am. Chem. Soc.* **1999**, *121*, 1226–1236.
[31] a) F. Effenberger, F. Wurthner, F. Steybe, *J. Org. Chem.* **1995**, *60*, 2082–2091; b) C. Reichardt, *Chem. Rev.* **1994**, *94*, 2319–2358.
[32] P. Garcia, J. M. Pernaut, P. Hapiot, V. Wintgens, P. Valat, F. Garnier, D. Delabouglise, *J. Phys. Chem.* **1993**, *97*, 513–516.
[33] S. A. Jenekhe, L. Lu, M. M. Alam, *Macromolecules* **2001**, *34*, 7315–7324.
[34] P. Suppan, N. Ghoneim, *Solvatochromism*, The Royal Society of Chemistry, Cambridge, **1997**.
[35] a) A. M. Sarker, B. Strehmel, D. C. Neckers, *Macromolecules* **1999**, *32*, 7409–7413; b) R. D. Schulte, J. F. Kauffman, *Appl. Spectrosc.* **1995**, *49*, 31–39.
[36] a) J. A. Osaheni, S. A. Jenekhe, *Macromolecules* **1994**, *27*, 739–742; b) B. Valeur, *Molecular Fluorescence: Principles and Application*, Wiley-VCH, Weinheim, **2002**; c) T. Förster, *Angew. Chem.* **1969**, *81*, 364–374; *Angew. Chem. Int. Ed. Engl.* **1969**, *8*, 333–343.
[37] J. Guillet, *Polymer Photophysics and Photochemistry*, Cambridge University Press, Cambridge, **1985**.
[38] a) L. J. Andrew, A. Deroulede, H. Linschitz, *J. Phys. Chem.* **1978**, *82*, 2304–2309; b) L. Biczók, T. Bérces, *J. Phys. Chem.* **1988**, *92*, 3842–3845; c) L. Biczók, T. Bérces, F. Márta, *J. Phys. Chem.* **1993**, *97*, 8895–8899; d) R. S. Murphy, C. P. Moorlay, W. H. Green, C. Bohne, *J. Photochem. Photobiol. A* **1997**, *110*, 123–129; e) S. A. Rani, J. Sobhanadri, T. A. P. Rao, *J. Photochem. Photobiol. A* **1996**, *94*, 1–5; f) S. A. Rani, J. Sobhanadri, T. A. P. Rao, *Spectrochim. Acta Part A* **1995**, *51*, 2473–2479.
[39] a) J. L. Brédas, R. Silbey, D. S. Boudreaux, R. R. Chance, *J. Am. Chem. Soc.* **1983**, *105*, 6555–6559; b) S. Janietz, D. D. C. Bradley, M. Greil, C. Giebeler, M. Inbasekaran, E. P. Woo, *Appl. Phys. Lett.* **1998**, *73*, 2453–2455; c) C. Chi, G. Wegner unpublished results.
[40] X. H. Yang, F. Jaiser, D. Neher, P. V. Lawson, J.-L. Brédas, E. Zojer, R. Güntner, P. S. de Freitas, M. Forster, U. Scherf, *Adv. Funct. Mater.* **2004**, *14*, 1097–1103.
[41] a) A. Elschner, R. F. Mahrt, L. Pautmeier, H. Bässler, M. Stolka, K. McGrane, *Chem. Phys.* **1991**, *150*, 81–91; b) S. C. J. Meskers, J. Hübner, M. Oestreich, H. Bässler, *Chem. Phys. Lett.* **2001**, *339*, 223–228.
[42] a) T. Förster, *Discuss. Faraday Soc.* **1959**, *27*, 7–17; b) J. R. Lakowicz, *Principles of Fluorescence Spectroscopy*, Plenum, New York, **1999**.

Received: March 11, 2005
Published online: August 31, 2005

